

# Effect of the coupling guide cross section on transmission and reflection mechanisms in a ramified acoustic system: theoretical analysis and COMSOL validation

Ilham El-Atmani<sup>1</sup>, Imane Chaker<sup>1</sup>, Aissam Khaled<sup>1,2</sup>, Driss Bria<sup>1</sup>, Moussed ech cherif el kettani<sup>2</sup> and Pierre Marechal<sup>3</sup>

<sup>1</sup>Laboratory of Materials, Waves, Energy and Environment, Team of Acoustics, Photonics and Materials, Faculty of Sciences, Mohamed Frist University, Oujda, Morocco

<sup>2</sup>Laboratory of Engineering Sciences and Applications ENSA Alhoceima, Morocco

<sup>3</sup>Laboratory of Waves and Complex Media, University Le Havre Normandy, France

**Abstract.** In this study, we examine the propagation of acoustic waves in a multichannel waveguide system composed of an input waveguide with a cross section  $S_0$  that corresponds to  $S_{Ref}$  and three output channels with cross sections  $S_1$ ,  $S_2$ , and  $S_3$  connected by a central coupling waveguide of length  $d_c$  and a cross section  $S_c$ . The study focuses on analyzing the transmission and reflection rates as a function of the cross-section  $S_c$  of the central guide. The theoretical results are validated through numerical simulations performed using COMSOL Multiphysics, showing excellent agreement between the analytical predictions and the simulation results. A very good agreement is obtained between theory and numerical simulations, confirming the accuracy of the proposed model. The results demonstrate the ability to control and adjust acoustic transmission paths by modifying the geometric parameters of the ramified system.

## 1 Introduction

The manipulation and control of acoustic wave propagation in waveguide systems have advanced significantly in recent years due to their potential uses in wave routing, signal processing, and acoustic communications [1–4]. Structured acoustic systems, particularly those combining waveguides and resonant structures, enable complex phenomena such as resonant transmission, acoustic transparency, and selective wave routing [5–7].

The propagation of acoustic waves in waveguides has therefore been studied extensively, with a strong focus on transmission and reflection characteristics. Initial theoretical studies by Pierce et al. [8] established analytical models describing wave interactions with interfaces, discontinuities, and impedance variations in tubes and ducts. Later, Kinsler et al [9] developed theoretical tools for predicting transmission and reflection coefficients in waveguides with various geometries and terminations. More recently, Sheng et al. [10] investigated wave scattering and transmission control in acoustic metamaterials and periodic waveguides, demonstrating how artificially engineered subwavelength structures can profoundly modify the flow of acoustic energy. The study therefore provides a fundamental understanding of how structured metamaterial based waveguides can be used as powerful platforms for manipulating acoustic energy. In addition, Afzal et al. [11] showed that even variations in the cross section of an elastic waveguide can significantly redistribute acoustic energy, strongly affecting scattering as well as the reflected, transmitted, and mode-coupled components. Such geometric

perturbations modify the balance between forward and backward waves and introduce additional interactions between different modes. This study emphasizes that when predicting or controlling acoustic wave propagation, one must consider the high sensitivity of elastic waveguides to geometric alterations. Wang et al. [12] demonstrated that periodically stubbed waveguides make it possible to adjust spectral gaps and control transmission by optimizing the geometry and spacing of the stubs. Their results indicated that the periodic addition of side branches acts similarly to a phononic crystal, creating band gaps through Bragg scattering and local resonances, and thus enabling precise manipulation of the frequencies allowed to pass through the waveguide.

Furthermore, Mei et al. [13] presented how surface acoustic waves (SAWs) can be guided, confined, and controlled in microscale acoustofluidic platforms. Their work highlighted how specially designed waveguides and microstructures can direct SAWs with high precision, enabling efficient fluid manipulation, particle transport, and localized energy concentration in devices.

Following these advances, recent research has increasingly explored complex waveguide architectures designed to control and manipulate acoustic wave propagation with high precision. Notably, structures such as splitters, couplers, and multibranch multiplexers [14–16] have their potential for compact, tunable, and highly selective routing of acoustic waves. For example, Similarly, Yin et al. [17] examined the coupling effects in parallel layered acoustic waveguides (PCAWs). Using a comprehensive approach that integrates mode

coupling theory, eigenmode analysis, and finite element simulations, they demonstrated how interactions between adjacent waveguides can be engineered to adjust transmission properties, suppress unwanted modes, and improve wave distribution across parallel channels. Moreover, William M. Robertson et al. [18] used numerical modelling and experiments to demonstrate how acoustic ring resonator structures can be used to manipulate audio-frequency acoustic waves. Three ring resonator systems are presented: a sequential array of identically spaced rings that generates acoustic bandgaps, a single ring between two parallel waveguides that functions as a filter, and a simple single ring construction that functions as a comb/notch filter. They used the impulse response method to perform tests in linear waveguides, 3D printing to construct the ring resonators, and COMSOL to perform numerical finite element simulations.

Moreover, William M. Robertson et al. [19] used numerical modelling and experiments to demonstrate how acoustic ring waveguide structures (loop) can be employed to manipulate audio-frequency acoustic waves. Three ring waveguide systems were presented: a sequential array of identically spaced rings generating acoustic bandgaps, a single ring waveguide coupled to two parallel waveguides functioning as a filter, and a simple single ring waveguide configuration acting as a comb/notch filter. The authors employed the impulse response method to perform measurements in linear waveguides, used 3D printing to fabricate the ring waveguides, and relied on COMSOL to carry out numerical finite element simulations.

In our present study, we investigate a multichannel acoustic waveguide system with one input guide and three output channels connected through a central coupling waveguide. The device distributes acoustic waves to the output channels depending primarily on the geometric parameters of the coupling guide, particularly its length  $d_c$  and cross section  $S_c$ . To analyze this behavior, we employ the transfer matrix method (TMM), which offers a clear understanding of how variations in the coupling section influence transmission rates in each channel. Complementary numerical simulations carried out using COMSOL multiphysics validate the theoretical predictions, showing strong agreement between analytical and numerical results. These findings confirm that the proposed structure enables effective control of acoustic wave transmission across multiple channels and thus provides a promising basis for configurable wave routing in designed acoustic systems.

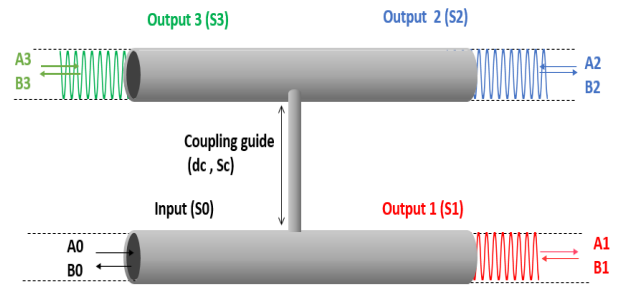


**Fig. 1.** Acoustic ramified system based on waveguide composed of input line of section  $S_0$  and three output channels with  $S_1, S_2$  and  $S_3$  sections.

## 2 Theoretical and numerical simulations

### 2.1 Theoretical model: transfer matrix method

The acoustic structure presented in **Fig. 1** is a ramified acoustic wave system consisting of one input channel of section  $S_0$  and three output channels of section  $S_i$  ( $i = \{1, 2, 3\}$ ) connected through a central coupling waveguide of length  $d_c$  and section  $S_c$ . Each output line  $i$  with ( $i = \{1, 2, 3\}$ ) is connected to a semi-infinite guide. In this context,  $\rho_0 = 1.2 \text{ Kg / m}^3$  represents the density of air, while  $c = 343.21 \text{ m / s}$  represents the speed of sound in air. All waveguides are characterized by the impedance  $Z = \rho c/S$  where  $S$  denotes the cross-section area of each guide. The method of calculation used in this study is based on the Transfer Matrix Method (TMM), used to solve the problem of the propagation of acoustic waves. This method enables us to obtain different physical properties of the studied system, such as the transmission and reflection rates.

We assume that a plane acoustic wave  $P_0(x)$  enters on the device from the left, expressed as:

$$P_0(x) = A_0 e^{jkx} + B_0 e^{-jkx} \quad (1)$$

where  $A_0$  and  $B_0$  denote the amplitudes of the incident and reflected waves, respectively. Here,  $k = \frac{\omega}{c}$  is the wavenumber in air. The corresponding particle velocity field is given by

$$V_0 = -\frac{1}{z_0} \nabla P \quad (2)$$

At each input and output of the ramified system, specific acoustic pressure and particle velocity fields are defined to characterize the propagation of waves within the structure:

$$\begin{cases} P_0(x) = A_0 e^{ikx} + B_0 e^{-ikx} \\ P_1(x) = A_1 e^{ikx} + B_1 e^{-ikx} \\ P_2(x) = A_2 e^{ikx} + B_2 e^{-ikx} \\ P_3(x) = A_3 e^{ikx} + B_3 e^{-ikx} \end{cases} \quad (3)$$

$$\begin{cases} V_0(x) = -\frac{1}{z_0} (A_0 e^{ikx} - B_0 e^{-ikx}) \\ V_c(y) = -\frac{1}{z_c} (A_c e^{iky} - B_c e^{-iky}) \\ V_1(x) = -\frac{1}{z_1} (A_1 e^{ikx} - B_1 e^{-ikx}) \\ V_2(x) = -\frac{1}{z_2} (A_2 e^{ikx} - B_2 e^{-ikx}) \\ V_3(x) = -\frac{1}{z_3} (A_3 e^{ikx} - B_3 e^{-ikx}) \end{cases} \quad (4)$$

$A_i$  ( $i = 0, 1, 2, 3$ ) are the amplitudes of the progressive acoustic waves in the 4 channels.

$B_i$  ( $i = 0, 1, 2, 3$ ) are the amplitudes of the regressive acoustic waves in the 4 channels with  $z_i = \frac{\rho c}{S}$ ,  $\rho$  and  $c$  are the density and speed of sound in air. It can be shown analytically that the transmission 2 through the output channel 2 and the transmission 3 through the channel 3 are equal.

We define  $a_{ij}$  as the elements of the matrix obtained by applying Hooke's laws as well as the continuity conditions on the expressions of pressure and velocity for an acoustic wave passing through the acoustic ramified waves. The transfer matrix of our proposed system allows us to relate the amplitudes of the incoming wave and the amplitudes of the outgoing wave :

$$\begin{pmatrix} A_0 \\ B_0 \end{pmatrix} = \begin{pmatrix} a_{11} & a_{12} & a_{13} & a_{14} & a_{15} & a_{16} \\ a_{21} & a_{22} & a_{23} & a_{24} & a_{25} & a_{26} \end{pmatrix} \begin{pmatrix} A_1 \\ B_1 \\ A_2 \\ B_2 \\ A_3 \\ B_3 \end{pmatrix} \quad (5)$$

The transmission and reflection coefficients are calculated by the following relations:

$$\begin{cases} t_1 = \frac{A_1}{A_0} \Big|_{B_1=0, B_2=0, B_3=0} ; t_2 = \frac{A_2}{A_0} \Big|_{B_1=0, B_2=0, B_3=0} \\ t_3 = \frac{A_3}{A_0} \Big|_{B_1=0, B_2=0, B_3=0} ; r = \frac{B_0}{A_0} \Big|_{B_1=0, B_2=0, B_3=0} \end{cases} \quad (6)$$

With:  $t_2 = t_3$ .

After a calculation, we can show that:

$$\begin{cases} t_1 = \frac{a_{23} + a_{25} + (a_{23} + a_{25})}{(a_{13} + a_{15})(e^{ik} - a_{21}) + a_{11}(a_{23} + a_{25})} \\ t_2 = \frac{(a_{21} - e^{ik}) + a_{11} e^{ik}}{(a_{23} + a_{25})(a_{21} - e^{ik}) - a_{11}(a_{23} + a_{25})} \\ r = [t_1 - e^{ik}] e^{ik} \end{cases} \quad (7)$$

The transmission rates in the output lines are given by:

$$T_1 = |t_1|^2 ; T_2 = |t_2|^2 ; T_3 = |t_3|^2 \quad (8)$$

The reflection rate in the input line is given by:

$$R = |r|^2 \quad (9)$$

The reflection and transmission rates satisfy the energy conservation:

$$R + T_1 + T_2 + T_3 = 1 \quad (10)$$

## 2.2 Numerical Simulations Using Finite Element Method in COMSOL

As part of the numerical modelling performed in COMSOL Multiphysics, acoustic excitation was applied via the entrance of the input line, using a pressure amplitude set to 1 Pa, with the ambient temperature set to 293.15 K. The entire model is based on the sound pressure interface in the frequency domain, and the linear acoustics module is considered throughout the simulation process. In this context, the problem is simplified by focusing on the system's acoustic response while practically neglecting the fluid's dynamic effects on wave propagation. To model acoustic wave propagation in our system, the Helmholtz equation is employed, taking into account the fluid density ( $\rho$ ) and acoustic pressure sources  $P$  [20].

By systematically modifying the cross section of the coupling section, the impact on the transmission rates to each output branch is studied. The numerical results provide a detailed validation of the predictions of the TMM and offer a visual representation of the spatial distribution of acoustic waves within the system.

**Table 1.** Characteristics of the Finite Element Method COMSOL to modeling the ramified system.

Aspect	Description
Geometry	One input waveguide ( $S_0 = S_{Ref}$ ) central coupling guide (variable cross-section $S_c$ , Length $d_c$ ) Three output channels (sections $S_1, S_2, S_3$ )
Boundary Conditions	Rigid walls for all waveguide boundaries Harmonic pressure source at the input
Frequency Range	0.01 Hz – 1000 Hz
Parameter Variation	Variation of the cross section and length of the Coupling guide to study their effect on transmission and reflection rates.
Outputs	Transmission rates ( $T_1, T_2, T_3$ ) ; Spatial pressure fields distributions
Purpose	Validate TMM predictions; analyze the effect of the coupling section geometry on acoustic waves splitting; visualize pressure distribution in the system

### 3 Results and discussions

#### 3.1 Spectra of transmission and reflection rates: effect of the coupling guide length $d_c$ and cross section $S_c$

In this subsection, we analyze the theoretical and numerical results of transmission rates  $T_1$ ,  $T_2$ ,  $T_3$  and reflection rate  $R$  as a function of frequency (Hz) for various values of the cross-section  $S_c$  of the coupling waveguide.

Different values of the coupling-guide cross section  $S_c$  are considered, namely  $S_c = S_{Ref}$ ,  $S_c = 0.75 S_{Ref}$ ,  $S_c = 0.5 S_{Ref}$ , and  $S_c = 0.1 S_{Ref}$ , which are represented by the red, green, blue, and black curves, respectively. The simulations are performed for a coupling guide of length  $d_c = 0.5$  m (Fig. 2 (a–d)) and an input cross section  $S_0 = S_{Ref}$ .

The solid curves illustrate the theoretical predictions obtained using the TMM, while the dotted curves represent the FEM results computed with COMSOL, showing excellent agreement between theory and numerical simulation. As  $S_c$  decreases, the transmission to channel 1 increases significantly;  $T_1$  increases from about 0.65 for  $S_c = S_0 = S_{Ref}$  to nearly 1 when  $S_c = 0.1 S_{Ref}$ . This means that almost all of the transmission goes into channel 1. At the same time,  $T_2$ ,  $T_3$ , and  $R$  gradually decrease toward zero, indicating that almost all the acoustic waves are directed into output channel 1. This behavior is explained by the reduction in the cross section of the guide  $d_c$ , which increases the acoustic impedance, directing most of the acoustic waves toward channel 1 (ON state) while greatly reducing the waves propagating toward channels 2 and 3 (OFF state).

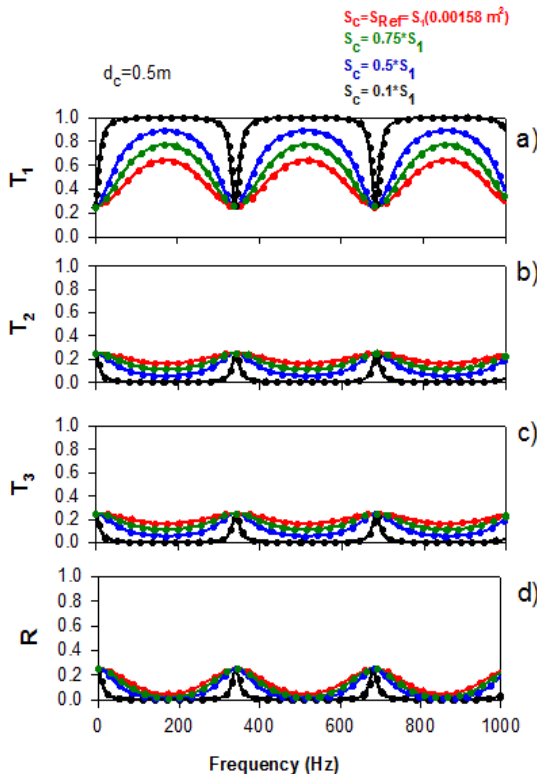


Fig. 2. Transmission and reflection rates as a function of frequency (Hz) for different values of the cross section ratio

$S_c/S_{Ref}$  for . Results are shown for  $S_c = S_{Ref}$ ,  $0.75S_{Ref}$ ,  $0.5S_{Ref}$ , and  $0.1S_{Ref}$  for  $d_c = 0.5$  m. TMM (solid) vs COMSOL (dotted).

The graph of Fig. 3(e–h) shows how the transmission rates  $T_1$ ,  $T_2$ ,  $T_3$ , and the reflection rate  $R$  change with frequency (Hz) for a coupling guide of length  $d_c = 1$  m. As in the previous analysis, the red, green, blue, and black curves correspond to  $S_c = S_{Ref}$ ,  $S_c = 0.75S_{Ref}$ ,  $S_c = 0.5S_{Ref}$ , and  $S_c = 0.1S_{Ref}$ , respectively. As in the case where  $d_c = 0.5$  m, we observe that reducing the cross section again favors transmission to channel 1, with  $T_1$  approaching unity for the smallest value,  $S_c = 0.1S_{Ref}$ , while  $T_2$ ,  $T_3$ , and  $R$  tend towards zero. Nevertheless, compared to the previous configuration, the number of transmission peaks (resonant characteristics) approximately doubles. This phenomenon is due to the doubling of the guide length  $d_c$ , which generates additional standing wave resonances in the coupling zone. A longer guide supports more resonant modes, resulting in an increased number of frequency points where transmission peaks appear. These results demonstrate that the coupling length  $d_c$  not only influence transmission rate efficiency but also determines the spectral selectivity of the device, allowing it to switch between broadband behavior and multi-resonance filtering depending on the chosen geometry.

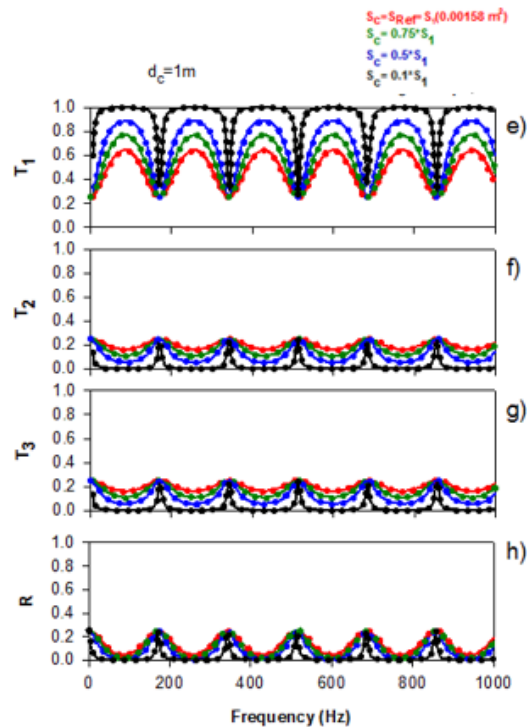
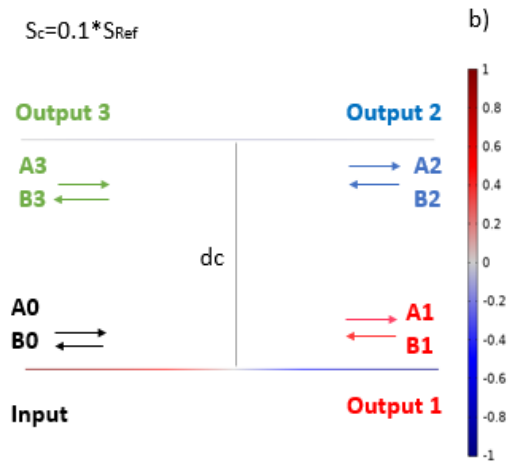
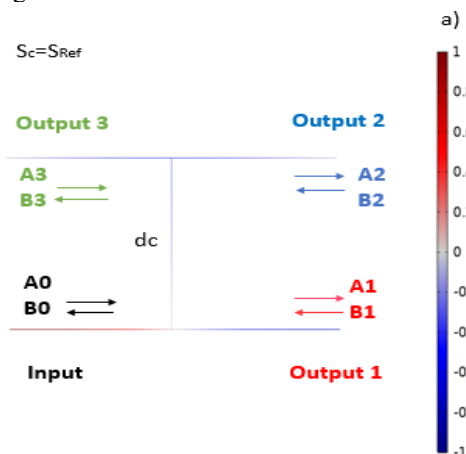


Fig. 3. Transmission and reflection rates as a function of frequency (Hz) for different values of the cross section ratio  $S_c/S_{Ref}$ . Results are shown for  $S_c = S_{Ref}$ ,  $0.75S_{Ref}$ ,  $0.5S_{Ref}$ , and  $0.1S_{Ref}$  for  $d_c = 0.5$  m. TMM (solid) vs COMSOL (dotted), with  $d_c = 1$  m. TMM (solid) vs COMSOL (dotted).

### 3.2 Distribution of the acoustic pressure field through the input and three output channels for different coupling cross sections $S_c$

In this part, Fig. 4 shows the total sound pressure level distribution along our acoustic system at two different values of the cross sections  $S_c$  of the coupling guide. We selected a representative frequency ( $f = 170.09$  Hz), which corresponds to the maximum peak of transmission rate  $T_1$  and minimum of transmissions  $T_2$ ,  $T_3$  and reflection rates  $R$  ((Fig. 2(a)). The acoustic pressure field at this frequency is presented in Fig. 4 (a-b) for a fixed coupling guide of length  $d_c = 0.5$  m with two values of  $S_c$ . When  $S_c = S_{Ref}$  (Fig. 4(a)) the pressure field shows a nearly symmetric distribution of the acoustic pressure, meaning that the acoustic wave is almost uniformly divided into the three output channels. In contrast, when the coupling section is reduced to a smaller value such as  $0.1S_{Ref}$  (Fig. 4(b)), the wave is almost entirely directed towards output channel 1, and the pressure amplitude is concentrated almost exclusively in this output channel. In this branch, the pressure map shows a strong dark blue color, which means the pressure is strongly negative. Output channels 2 and 3 also appear mostly in blue, showing low and negative pressure levels.

In summary, when the coupling section  $S_c$  is large, the acoustic wave spreads across the three output channels. When  $S_c$  becomes smaller, almost all the wave is directed to output channel 1, acting as an acoustic switch. Thus,  $S_c$  controls the wave distribution, enabling a transition from a multichannel power divider to a single-channel switch.



**Fig. 4.** Acoustic pressure field distributions (Pa) at  $f=170.09$  Hz for different coupling cross section areas  $S_c$  with a fixed coupling guide of length  $d_c=0.5$  m: (a)  $S_c=S_{Ref}$  and (b)  $S_c=0.1S_{Ref}$ .

### 3.3 Effect of the coupling section ratio $S_c/S_{Ref}$ on the maximum of transmission and reflection rates

This subsection investigates the effect of the cross-section ratio  $S_c/S_{Ref}$  of the coupling waveguide of length  $d_c$  on the maximum transmission  $T_1$ ,  $T_2$ ,  $T_3$  and reflection  $R$  rates. In this case, the cross section of the coupling guide is denoted by  $S_c$ , and the input guide by  $S_0=S_{Ref}$ . The fig. 5 shows the evolution of the maximum values of the transmission rates  $T_1$ ,  $T_2$ ,  $T_3$  as well as the reflection rate  $R$  as a function of the ratio  $S_c/S_{Ref}$ . As shown in Fig. 5, when  $S_c/S_{Ref}$  increases,  $T_1$  gradually decreases, going from 1 for minimal cross-sections to around 0.64 when  $S_c = S_{Ref}$ .

On the other hand,  $T_2$ ,  $T_3$ , and  $R$  increase as the ratio  $S_c/S_{Ref}$  becomes larger until they reach a limit value corresponding to a critical section  $S_{Critique}$ , after which these rates remain practically constant even if  $S_c/S_{Ref}$  continues to increase.

This behavior illustrates the influence of the geometric coupling between the input and output channels; increasing the coupling section increases the interaction between the guides, creating wave transfer to outputs 2 and 3 channels while reducing it in the first output channel.

The increase in reflection rate  $R$  results from changes in the pressure field at the coupling junction of the guide, which modify the impedance and cause partial reflection of the incident wave. When the critical section is reached, the system becomes stable, and the coupling reaches its highest point. At this point, the wave's distribution between the channels is no longer affected by  $S_c$ .

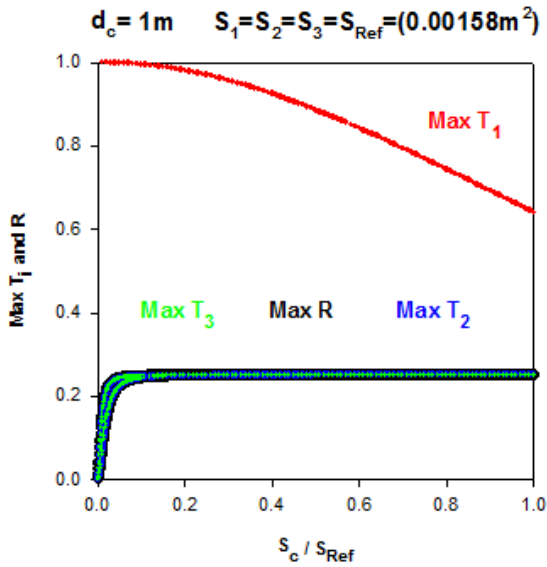


Fig. 5. Evolution of transmission maxima  $T_1$ ,  $T_2$ ,  $T_3$  and reflection maximum  $R$  as a function of  $S_c/S_{\text{Ref}}$  with  $d_c = 1\text{m}$ .

### 3.4 Effect of the coupling section ratio $S_c/S_{\text{Ref}}$ on the frequencies of transmission and reflection Maxima through the input and three output Channels

In this part, we examine the evolution of the resonance frequencies corresponding to the maxima transmissions and reflection rates  $T_1$ ,  $T_2$ ,  $T_3$ , and  $R$  as a function of the cross-section ratio  $S_c/S_{\text{Ref}}$ . Fig. 6 illustrates the variation in transmission peaks for  $T_1$  (red color),  $T_2$  (blue color),  $T_3$  (green color), and  $R$  (black color) over the range ( $0 < d_c < 4\text{m}$ ).

The resonance frequencies associated with  $T_2$ ,  $T_3$ , and reflection  $R$  coincide and appear at the same frequency positions, while those of  $T_1$  appear at slightly different frequencies. The difference for ( $T_1$ ) reflects a redistribution of the waves between the input guide and the output channels. As the ratio ( $S_c/S_{\text{Ref}}$ ) increases, the coupling between the first output channel and the side branches modifies the modal structure, causing a variation in the effective acoustic path and, consequently, in the resonance frequencies.

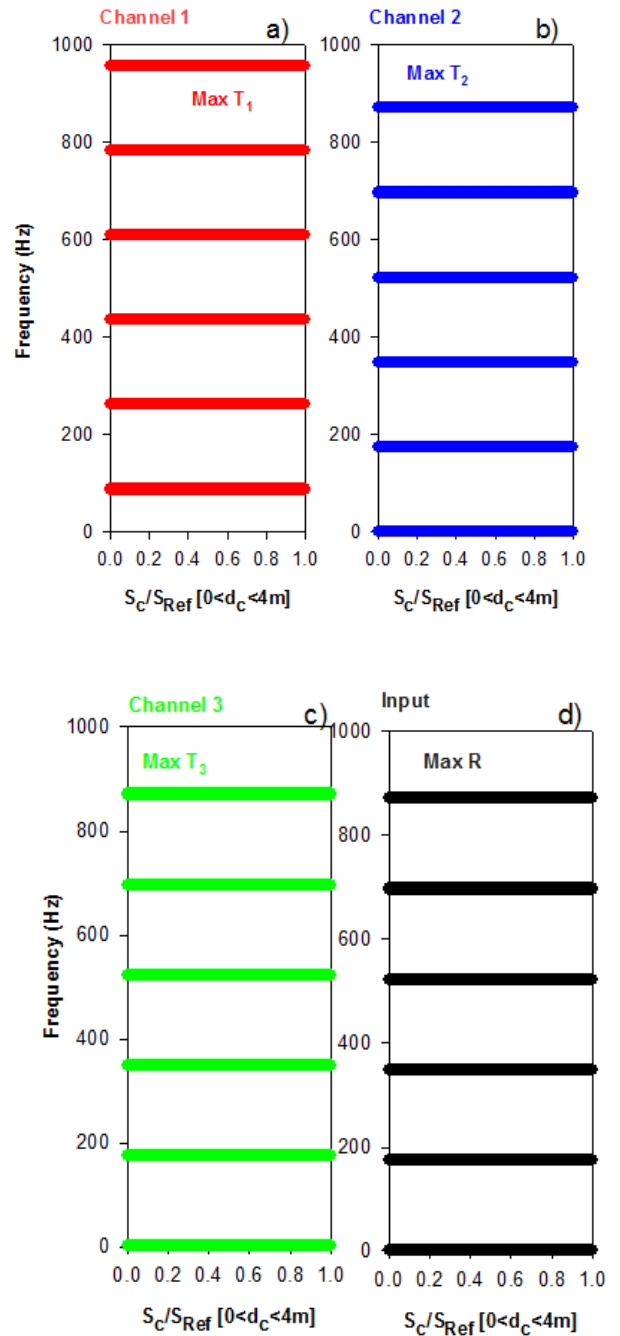


Fig. 6. Variation of the frequencies (Hz) corresponding to maxima of transmission and reflection rates as a function of the section ratio  $S_c/S_{\text{Ref}}$ : (a)  $T_1$  (red color), (b)  $T_2$  (blue color), (c)  $T_3$  (green color), and (d) reflection (black Color) for  $0 < d_c < 4\text{m}$ .

## 4 Conclusion

In this research, we explored the impact of the coupling section  $S_c$  on the transmission behavior of a ramified acoustic waveguide system. We showed, using the transfer matrix method and finite element method simulations, that the coupling section is essential for regulating the distribution of the acoustic waves between the output channels. The results indicate that as  $S_c$  decreases, the transmitted wave is mainly directed toward input channel 1, resulting in almost total wave

transmission at this output. Conversely, when  $S_c$  increases, the interference conditions are modified, allowing for a redistribution of acoustic waves between the different channels. The strong agreement between theoretical predictions and the FEM simulations confirms the reliability of the proposed model. These findings highlight the novelty and practical relevance of geometric control as a robust mechanism for acoustic switching, wave routing, and efficient management of acoustic energy in compact waveguide architectures.

**Acknowledgements:** We would like to express our sincere gratitude to the Laboratory of Materials, Waves, Energy and Environment and Laboratory of Waves and Complex Media for providing the facilities and scientific support that made this work possible. We also acknowledge the financial support of the CNRST (National Center for Scientific and Technical Research, Morocco) Under the doctoral research program. Their continuous assistance and encouragement were essential to the completion of this study.

## References

1. H. Teutsch, Modal array signal processing: principles and applications of acoustic wavefield decomposition. Berlin, Heidelberg: Springer Berlin Heidelberg (2007).  
[https://doi.org/10.1007/978-3-540-40896-3\\_4](https://doi.org/10.1007/978-3-540-40896-3_4)
2. J. Mei, J. Friend, A review: Controlling the propagation of surface acoustic waves via waveguides for potential use in acoustofluidics. Mechanical Engineering Reviews, 7(1), 19-00402 (2020).  
<https://doi.org/10.1299/mer.19-00402>
3. Z. X. Huang, H. W. Wu, L. L. Cheng, P. X. Xie, X. Chen, H. F. Xu, Z. Q. Sheng. Steering sound propagation with Zeno barriers in acoustic waveguide arrays. Applied Physics Letters, 125(15) (2024).  
<https://doi.org/10.1063/5.0234559>
4. A. M. Zelenyak, M. A., Hamstad, M. G. Sause. Modeling of acoustic emission signal propagation in waveguides. Sensors, 15(5), 11805-11822 (2015).  
<https://doi.org/10.3390/s150511805>
5. V., Achilleos, O., Richoux, G., Theocharis, D. J. Frantzeskakis. Acoustic solitons in waveguides with Helmholtz resonators: Transmission line approach. Physical Review E, 91(2), 023204 (2015).  
<https://doi.org/10.1103/PhysRevE.91.023204>
6. M. K., Schmidt, M. C., O'Brien, Steel, M. J., & Poulton, C. G. ARRAW: anti-resonant reflecting acoustic waveguides. New Journal of Physics, 22(5), 053011(2020).  
<https://doi.org/10.1088/1367-2630/ab7d79>
7. Y. Liu, N. Dostart, M. A. Popović. Toward microphononic circuits on chip: an evaluation of components based on high-contrast evanescent confinement of acoustic waves. arXiv preprint arXiv:1707.06280. (2017).  
<https://doi.org/10.48550/arXiv.1707.06280>
8. A. D. Pierce, Acoustics: an introduction to its physical principles and applications. Springer (2019).  
Book
9. L. E., Kinsler, A. R., Frey, A. B., Coppers, J. V. Sanders (Fundamentals of acoustics. John Wiley & sons (2000).  
Book
10. P., Sheng, X. X., Zhang, Z., Liu, & Chan, C. T. Locally resonant sonic materials. Physica B: Condensed Matter, 338(1-4), 201-205 (2003).  
[https://doi.org/10.1016/S09214526\(03\)00487-3](https://doi.org/10.1016/S09214526(03)00487-3)
11. M., Afzal, R., Nawaz, M., Ayub, & Wahab, A. Acoustic scattering in flexible waveguide involving step discontinuity. PloS one, 9(8), e103807 (2014).  
<https://doi.org/10.1371/journal.pone.0103807>
12. X. F., Wang, M. S., Kushwaha, & P. Vasilopoulos. Tunability of acoustic spectral gaps and transmission in periodically stubbed waveguides. Physical Review B, 65(3), 035107. (2001).  
<https://doi.org/10.1103/PhysRevB.65.035107>
13. J., Mei, & J. Friend. A review: Controlling the propagation of surface acoustic waves via waveguides for potential use in acoustofluidics. Mechanical Engineering Reviews, 7(1), 19-00402 (2020).  
<https://doi.org/10.1299/mer.19-00402>
14. F. Z., Berahioui, I., El-Atmani, Y., Errouas, A., Ouariach, F., Falyouni, D. Bria. I-Shaped Amplitude Divider Based on 1D Photonic System. In International Conference on Electronic Engineering and Renewable Energy Systems (pp. 55-63). Singapore: Springer Nature Singapore. (2024, May).  
Conference paper
15. T., Jamneala, M., Small, R., Ruby, J. D. Larson, Coupled resonator filter with single-layer acoustic coupler. IEEE transactions on ultrasonics, ferroelectrics, and frequency control, 55(10), 2320-2326 (2008).  
<https://doi.org/10.1109/TUFFC.931>
16. I., Chaker, Y., Errouas, I., El-Atmani, A., Ghaban, D., Bria, K. Laabidi, Y-Shaped Electromagnetic Switch Using Waveguides and a Resonator. In International Conference on Electronic Engineering and Renewable Energy Systems (pp. 153-163). Singapore : Springer Nature Singapore (2024, May).  
Conference paper
17. G., Yin, P., Li, X., Yang, Y., Tian, J., Han, W., Ren, J. Guo. Characteristics and mechanism of coupling effects in parallel-cladded acoustic waveguides. Acta Acustica, 6, 8(2022).  
<https://doi.org/10.1051/aacus/2022002>
18. W. M., Robertson, C., Vazquez, A., LaVerde, A., Wassenberg, C., Olson, J. Lopez, Acoustic ring

- resonator: Experiments and simulations. *AIP Advances*, 12(1) (2022).  
<https://doi.org/10.1063/5.0077330>
19. L., Yang, J., Zhang, J., Xia, S., Zhang, & Y. Yang. Sound transmission loss of helmholtz resonators with elastic bottom plate. *Sound & Vibration*, 58(1), 056968-056968 (2024).
  20. Y., El Chami, Z., Pezeshki, S. S., Mohamed, & B. Safaei. Enhanced acoustic attenuation performance of a novel absorptive muffler: A Helmholtz equation-based simulation study. *J. Eng. Manag. Syst. Eng*, 3(1), 53-64 (2024).  
<https://doi.org/10.56578/jemse030105>.